NANO LETTERS

2008
Vol. 8, No. 2
596−600

Size Limits on Doping Phosphorus into Silicon Nanocrystals

T.-L. Chan,[†] Murilo L. Tiago,[†,||] Efthimios Kaxiras,[‡] and James R. Chelikowsky*[,†,§]

Center for Computational Materials, Institute for Computational Engineering and Sciences, Departments of Physics and Chemical Engineering, University of Texas, Austin, Texas 78712, and Department of Physics and School of Engineering and Applied Sciences, Harvard University, Cambridge, Massachusetts 02138

Received November 16, 2007; Revised Manuscript Received December 11, 2007

ABSTRACT

We studied the electronic properties of phosphorus-doped silicon nanocrystals using the real-space first-principles pseudopotential method. We simulated nanocrystals with a diameter of up to 6 nm and made a direct comparison with experimental measurement for the first time for these systems. Our calculated size dependence of hyperfine splitting was in excellent agreement with experimental data. We also found a critical nanocrystal size below which we predicted that the dopant will be ejected to the surface.

Doping a small percentage of foreign atoms in bulk semiconductors can profoundly change their electronic properties and makes possible the creation of modern electronic devices.[1] Phosphorus doped into bulk Si introduces defect energy states close to the conduction band of Si. For such shallow donors, electrons can be easily thermally excited, thereby greatly enhancing the conductivity of the original pure semiconductor by orders of magnitude at room temperature. The evolution of the semiconductor industry requires continued miniaturization. Currently, the industry is maintaining exponential gains in performance of electronic circuits by designing devices ever smaller and denser than the previous generation. This device miniaturization will ultimately approach the nanometer scale. Thus, it is of the utmost importance to understand how doping operates at this length scale. Quantum confinement is expected to alter the electronic properties of doped Si nanocrystals.[2] Doped Si nanowires have also been synthesized and demonstrated experimentally that they can be used as interconnects in electronic circuits or building blocks for semiconductor nanodevices.[3,4] Important questions arise as to whether the defect energy levels are shallow or not, for example, at what length scale will device construction based on macroscopic laws fail?

Phosphorus-doped silicon nanocrystals represent the prototypical system for studying impurities in quantum dots. Recent experiments dedicated to studying this system have utilized photoluminescence[5,6] and electron spin resonance measurements.[7−9] The electron spin resonance experiments probe the defect energy levels through hyperfine interaction. Hyperfine splitting (HFS) arises from the interaction between the electron spin of the defect level and the nucleus spin, which is directly related to the dopant electron density localized on the impurity site.[10] A HFS much higher than the bulk value of 42 G has been observed for P-doped Si nanocrystals with radii of 10 nm.[7] A size dependence of the HFS of P atoms was also observed in Si nanocrystals.[8,9]

Unfortunately, theoretical studies of shallow impurities in quantum dots are still computationally challenging. Owing to the large number of atoms and to the low symmetry of the system involved, first-principles total energy calculations have been limited to studying nanocrystals that are much smaller than the size synthesized in experiment.[11−14] While empirical studies have been performed for impurities in large quantum dots, they often utilize parameters that are ad hoc extrapolations of bulklike values.[15−17]

In this work, we use a first-principles method to study the electronic properties of P-doped Si nanocrystals. Compared to previous first-principles studies, we perform calculations for P-doped Si nanocrystals up to a diameter of 6 nm, which spans the entire range of experimental measurements.[9] Our calculated HFS in P-doped Si nanocrystals is in excellent agreement with the experimentally measured size dependence. The HFS size dependence is a result of strong quantum confinement, which also leads to higher binding energy of the dopant electron. Hence P is not a shallow donor in Si if the nanocrystals are less than 20 nm in diameter. In addition, we found a "critical'' nanocrystal size below which

* Corresponding author. E-mail: jrc@ices.utexas.edu.
[†] Center for Computational Materials, Institute for Computational Engineering and Sciences, University of Texas.
[‡] Department of Physics and School of Engineering and Applied Sciences, Harvard University.
[§] Departments of Physics and Chemical Engineering, University of Texas.
[||] Present address: Materials Science and Technology Division, Oak Ridge National Laboratory, Oak Ridge, Tennessee 37831.

10.1021/nl072997a CCC: $40.75
Published on Web 12/23/2007

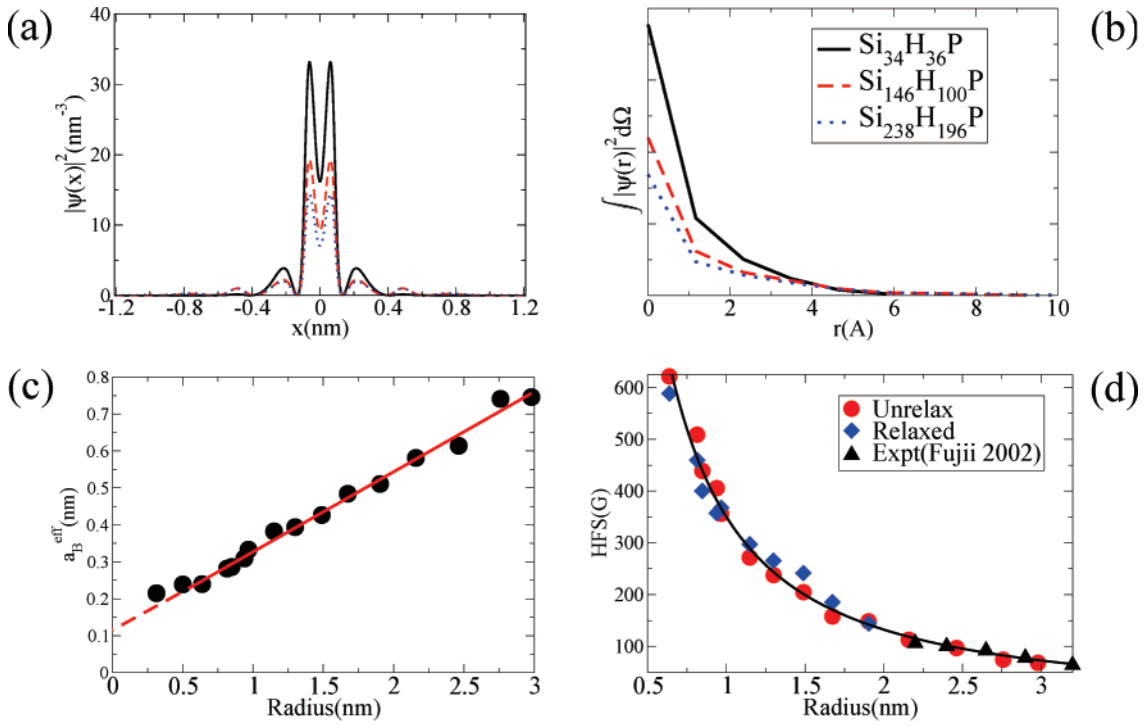

Figure 1. (a) Charge density for the dopant electron along the [100] direction for three P-doped Si nanocrystals with different radius. *x* is the coordinate along that direction. (b) The corresponding spherically averaged charge densities. (c) The effective Bohr radius a_B^{eff} corresponding to the dopant electron as a function of nanocrystal radius. (d) Calculated HFS of P-doped Si nanocrystals as a function of nanocrystal radius together with experimental data (▲) from ref 9. Theoretical values for both the unrelaxed bulk geometries (●) and the fully relaxed structures (◆) are shown.

the P donor is not stable against migration to the surface. We also provide a mapping from our first-principles calculations to a hydrogen-like quantum model, which provides a general procedure for modeling impurities in semiconductor nanostructures.

Our first-principles calculations are based on density functional theory in the local density approximation[18] using a real-space grid pseudopotential method. The grid spacing is chosen to be 0.03 nm; other details of our calculations can be found in ref 19. The geometry of Si nanocrystal is assumed to be bulklike and roughly spherical in shape in accord with experimental observation.[20] The dangling bonds on the surface of the nanocrystal are passivated by H. The experimentally synthesized Si nanocrystals are usually embedded in an amorphous silicon dioxide matrix. The Si/SiO_2 interface is in general not the same as H passivation. Nevertheless, both serve the role of satisfying the dangling bonds on the surface. The Si nanocrystals are then doped with one P atom, which substitutes a Si atom in the nanocrystal.

We first discuss the defect wavefunction in P-doped Si nanocrystals. In Figure 1a, we plot the defect state charge density along the [100] direction. We can see that as the nanocrystal size increases, the defect wavefunction becomes more delocalized. This quantum confinement effect is observed in both experiments[9] and theoretical calculations.[11,21] The maxima of the charge density at around 0.2 nm correspond to the bond length between the P at the origin and its first Si neighbors. We can smooth out these atomic details by spherically averaging the defect wavefunction as shown in Figure 1b. We find that the defect wavefunction decays exponentially from the origin. This corresponds very well to the conventional understanding of defects in semiconductors: the defect ion and the defect electron form a hydrogen-like system with the wavefunction described as $\psi \sim exp(-r/a_B^{eff})$.

From the decay of the defect wavefunction, we can obtain an effective Bohr radius a_B^{eff} and its dependence on nanocrystal size as plotted in Figure 1c. We find that the effective Bohr radius varies nearly linearly with nanocrystal radius R up to 3 nm where R is approximately five times a_B^{eff}. Nonlinearity can be observed for very small Si nanocrystals, and a_B^{eff} appears to converge to ~0.2 nm as $R \rightarrow 0$. The limit trends to the size of a phosphorus atom while retaining its sp^3 hybridization. In the bulk limit, a_B^{eff} is ~2.3 nm assuming a dielectric constant of 11.4 and effective electron mass of 0.26 m_e. Therefore, the dependence on R should trend to this bulk limit when the diameter of the nanocrystal is sufficiently large, which is outside of the size regime shown in our figure.

From the defect wavefunctions, we can evaluate the isotropic HFS as well.[22,23] Our calculated HFS is plotted in Figure 1d for a P atom located at the center of Si nanocrystal. There is very good agreement between experimental data[9] and our theoretical calculations. For nanocrystals with a radius between 2 and 3 nm, the HFS is around 100 G, which considerably exceeds the bulk value of 42 G. Moreover, the HFS continues to increase as the nanocrystal size decreases. This is a consequence of the quantum confinement as illustrated in Figure 1a,b. The defect wavefunction becomes

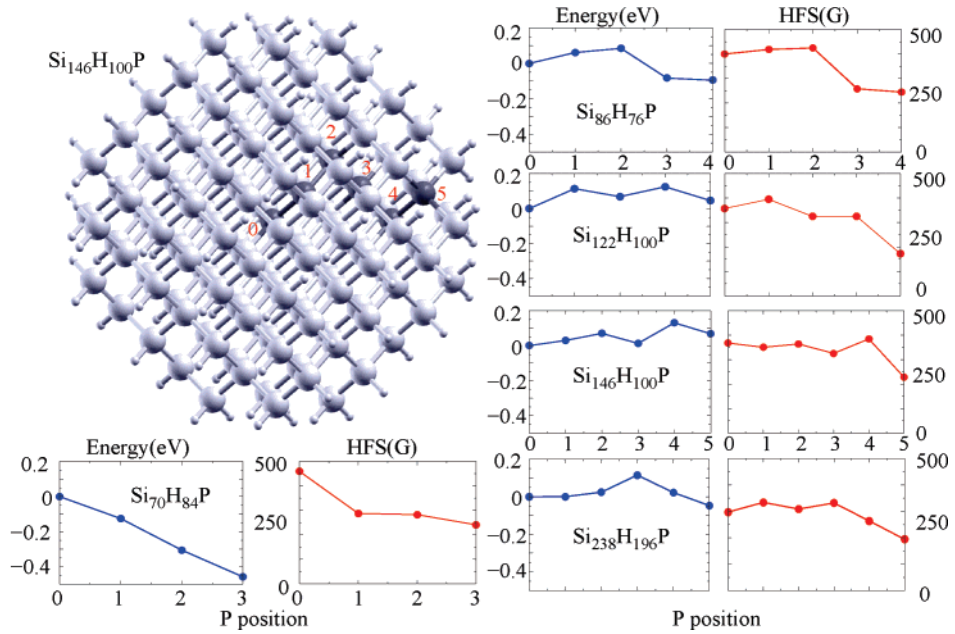

Figure 2. Difference in energy and HFS as the P atom moves away from the center of the Si nanocrystal. The energies are with respect to the energy of the Si nanocrystal with P at the center. The *x*-axis measures the distance of P atom away from the origin in the unit of Si bond length as illustrated in the perspective view of a Si nanocrystal.

more localized at the P site as the radius decreases, leading to higher amplitude of the wavefunction at the P core. Owing to heavy computational cost, only Si nanocrystals containing less than 1500 Si atoms are structurally optimized to a local energy minimum. However, for Si nanocrystals with a radius larger than 1.5 nm, the effect of relaxation diminishes and the difference between unrelaxed and relaxed results is within ~10% .

The experimental methodology used to measure the HFS ensures that only nanocrystals with exactly one impurity atom are probed. However, experiment has no control over the location of the impurity within the nanocrystal. The spatial distribution of impurities cannot be inferred from experimental data alone. Therefore, we considered the energetics of the doped nanocrystal by varying the P position along the [100] direction as illustrated in Figure 2. We avoid substituting the Si atoms on the surface of the nanocrystal by P. Our results for five of the small nanocrystals after relaxation to local energy minimum are shown in Figure 2. For Si nanocrystals with a diameter smaller than ~2 nm, P tends to substitute Si near the surface. Otherwise, there is a bistable behavior in which both the center and the surface of the nanocrystal are energetically stable positions. This suggests that a "critical size'' exists for nanocrystals. Below this size, P atoms will always be energetically expelled toward the surface.

To understand this phenomenon, we calculated the binding energy E_B of the defect electron as the P position changes. The binding energy is a measure of how strongly the defect electron interacts with the P atom and is calculated by the energy required to ionize a P-doped Si nanocrystal by removing an electron (I_d) minus the energy gained by adding the electron to a pure Si nanocrystal (A_p). Figure 3a illustrates the typical situation for Si nanocrystals larger than 2 nm in diameter: the binding energy tends to decrease as the P moves toward the surface. This is owing to the defect wavefunction becoming more distorted and less localized around P, leading to a loss in Coulomb energy between the P ion and the defect electron. This explains why the center of the nanocrystal is energetically favorable. However, because the doped nanocrystal can relieve its stress by expelling the P atom toward the surface where there is more room for relaxation, positions close to the surface are always locally stable as depicted in Figure 2. Therefore, the binding energy and P-induced stress compete with each other in determining the defect position within the Si nanocrystal.

On the other hand, for Si nanocrystals less than 2 nm in diameter the binding energy is higher close to the surface of the Si nanocrystal as shown in Figure 3b,c. A comparison of the binding energy between relaxed and unrelaxed structures suggests that the reversal in the trend is caused by relaxation. From Figure 3e, the P atom is found to relax toward the center of the nanocrystal, leading to a more localized defect wavefunction as in Figure 3d with better confinement inside the nanocrystal and therefore higher binding energy. The relaxation of P atom toward the center of the nanocrystal causes an expansion of the Si nanocrystal in the perpendicular direction creating strain throughout the nanocrystal. This tradeoff between the binding energy and stress is only feasible for small Si nanocrystals as depicted in Figure 3f. As the diameter of the Si nanocrystal increases, the relaxation trends to a bulklike geometry. The interplay between the binding energy and stress for small Si nanocrystals stabilizes the P atom close to the surface of the nanocrystal.

The HFS evaluated for different P positions inside the Si nanocrystal is also shown in Figure 2. There is a general trend for the HFS to drop drastically as the P atom gets close to the surface of the nanocrystal. Smaller variations in the HFS are found for P positions away from the surface.

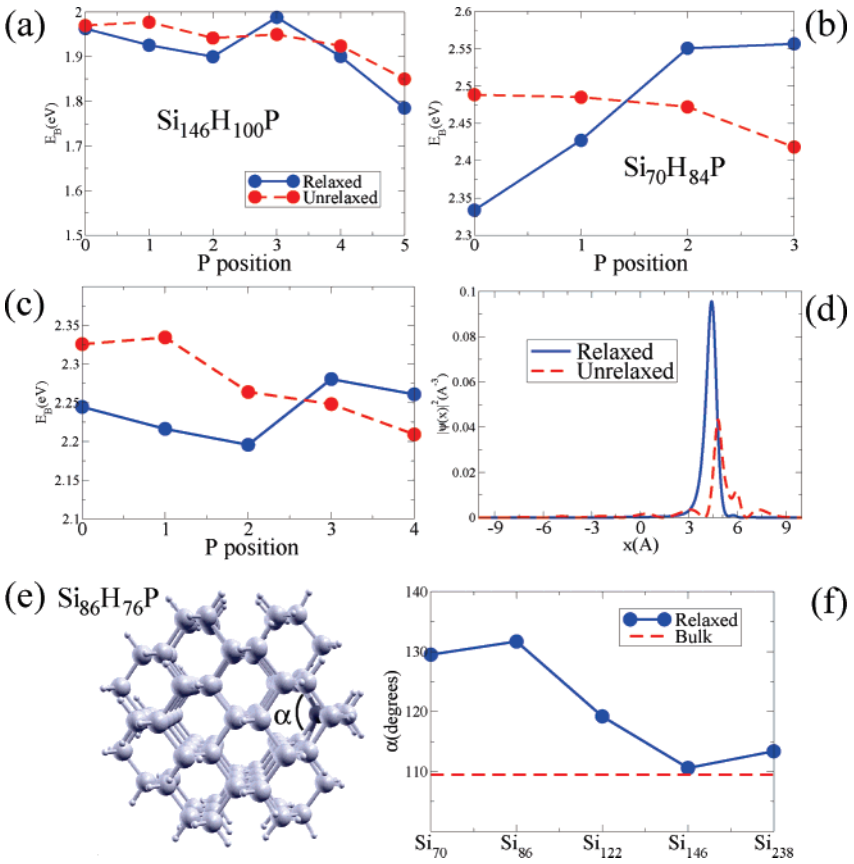

Figure 3. (a−c) Changes in binding energy as the P atom moves away from the center of three Si nanocrystals with different size. The same *x*-axis is used as in Figure 2. (d) The charge density of the dopant electron along the [100] direction (*x* direction) for the $Si_{86}H_{76}P$ cluster with the P atom located close to the surface as illustrated in (e). (f) A plot of the angle subtended by the P atom located close to the surface for five different Si nanocrystals. Only the number of Si atoms is used to label the *x*-axis for clarity. The solid line represents the results after relaxation, while the dashed line corresponds to unrelaxed bulklike geometries in the figure.

However, for a large Si nanocrystal the HFS varies within ~10% of the value with P at the center position. From our studies of the energetics and comparison to the experimental results in Figure 1d, it is possible for the synthesized Si nanocrystals to have P located close to the center of the nanocrystals.

Our analysis of the defect wavefunction in Figure 1 can be fitted to an effective mass model. Motivated by the defect wavefunctions having an approximate form of $\exp(-r/a_B)$, we consider a hydrogen-like atom in a "dielectric box''. The potential that the electron experiences in atomic unit is

$$V(r) = \begin{cases} \dfrac{-1}{\epsilon(R)r} + V_0 & \text{for } r \le R; \\ \dfrac{-1}{\epsilon(R)r} & \text{otherwise} \end{cases} \quad (1)$$

R is the radius of the well, and V_0 the well depth. The dielectric constant $\epsilon(R)$ depends on nanocrystal size[24] and is assumed to follow Penn's model $\epsilon(R) = 1 + (11.4 - 1)/(1 + (\alpha/R)^n)$.[25] The dielectric constant converges to 11.4 in the bulk limit. α and n will be used as fitting parameters. We obtain an approximate solution to the Schrodinger equation for the defect electron with an effective mass $m^* = 0.26\ m_e$ under this potential by using a trial wavefunction $\psi = \sqrt{\pi/a_B^3}\ \exp(-r/a_B)$. By applying the variational principle, the energy can be minimized with respect to the effective Bohr radius a_B. Hence, a_B can be found as a function of the well depth V_0 and radius R. Alternatively, V_0 can be inferred because we know a_B from our first-principles results. In fact, the energy calculated from this model corresponds to the binding energy E_B of the dopant electron. Therefore, we can fit the α and n parameters in Penn's model by calculating the binding energy. Our calculated size dependence of the binding energy ($E_B = I_d - A_p$ as defined above) is plotted in Figure 4a,b). A detailed explanation of the trend can be found in ref 11.

Figure 4 illustrates the results from the fitting to the effective mass model. By using α = 5.4 nm and n = 1.6, we find that our model can reproduce almost exactly the binding energies from the first-principles calculations. The binding energy E_B scales as $R^{-1.1}$, where R is the nanocrystal radius, is a manifestation of an admixture of several contributions. For nanocrystals up to 6 nm in diameter, the binding energy is significantly larger than k_BT at room temperature. An extrapolation of our results shows that a nanocrystal diameter of at least 20 nm is needed for P to be a shallow donor. Interestingly, the depth of the potential well V_0 depends on the nanocrystal radius R rather than being infinite or a constant. The finite V_0 explains the dependence

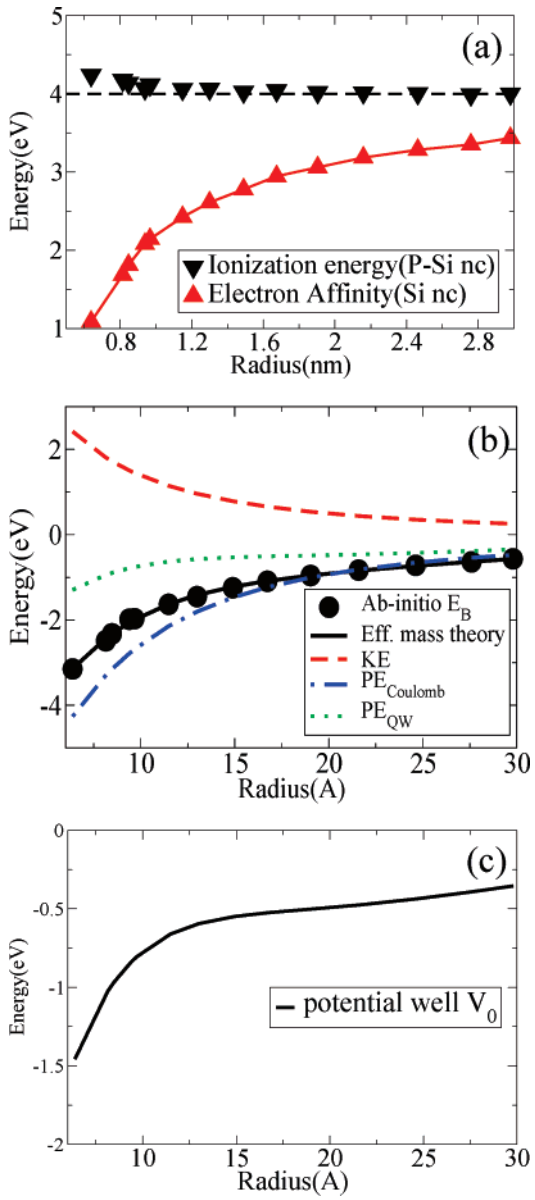

Figure 4. (a) Ionization energy of P-doped Si nanocrystal (▼) and electron affinity of pure Si nanocrystal (▲) plotted as a function of nanocrystal radius. (b) Calculated binding energy E_B using effective mass theory plotted together with our ab initio results. From effective mass theory, the binding energy has contributions from the kinetic energy (KE), the Coulomb interaction between the dopant ion and its electron ($PE_{Coulomb}$), and the potential energy (PE_{QW}) due to the quantum well. (c) The potential well depth V_0 as a function of nanocrystal radius from effective mass theory based on a hydrogen atom in a box.

of HFS on R scales with an exponent smaller than three, which is a consequence of an infinitely deep quantum well.[26] The well represents the effect of quantum confinement on the wave function, which for very large nanocrystals diminishes, corresponding to a vanishing quantum well in the bulk limit. As the nanocrystal size decreases, the quantum well becomes deeper such that it can confine the defect electron more effectively as its kinetic energy increases.

In summary, we studied the defect wavefunctions in P-doped Si nanocrystals with a diameter of up to 6 nm by first-principles calculations. Our calculated hyperfine splitting has very good agreement with experimental data. We found that the defect wavefunction has a functional form similar to the hydrogen 1s orbital. A model calculation of a hydrogen atom in a quantum well can be used to describe the defect electron. In addition, our study on the energetics of P location in the Si nanocrystals indicates that the P atom will be expelled toward the surface of the nanocrystal with a diameter below a critical value of ~2 nm.

Acknowledgment. This work was supported in part by the National Science Foundation under DMR-0551195 and the U.S. Department of Energy under DE-FG02-06ER46286 and DE-FG02-06ER15760. Computational resources were provided in part by the National Energy Research Scientific Computing Center (NERSC) and the Texas Advanced Computing Center (TACC).

References

(1) Streetman, B. G.; Banerjee, S. *Solid State Electronic Devices*, 5th ed. Prentice Hall: New Jersey, 2000.
(2) Yoffe, A. D. *Adv. Phys.* **2001**, *50*, 1.
(3) Cui, Y.; Lieber, C. M. *Science* **2001**, *291*, 851.
(4) Appell, D. *Nature* **2002**, *419*, 553.
(5) Mimura, A.; Fujii, M.; Hayashi, Sh.; Kovalev, D.; Koch, F. *Phys. Rev. B* **2000**, *62*, 12625.
(6) Mauckner, G.; Rebitzer, W.; Thonke, K.; Sauer, R. *Phys. Status Solidi B* **1999**, *215*, 871.
(7) Muller, J.; Finger, F.; Carius, R.; Wagner, H. *Phys. Rev. B* **1999**, *60*, 11666.
(8) Pawlak, B. J.; Gregorkiewicz, T.; Ammerlaan, C. A. J.; Takkenberg, W.; Tichelaar, F. D.; Alkemade, P. F. A. *Phys. Rev. B* **2001**, *64*, 115308.
(9) Fujii, M.; Mimura, A.; Hayashi, Sh.; Yamamoto, Y.; Murakami, K. **2002**, *89*, 206805.
(10) Feher, G. *Phys. Rev.* **1959**, *114*, 1219.
(11) (a) Melnikov, D. V.; Chelikowsky, J. R. *Phys. Rev. Lett.* **2004**, *92*, 46802. (b) Melnikov, D. V.; Chelikowsky, J. R. *Phys. Rev. B* **2004**, *69*, 113305.
(12) Zhou, Z.; Steigerwald, M. L.; Friesner, R. A.; Brus, L.; Hybertsen, M. S. *Phys. Rev. B* **2005**, *71*, 245308.
(13) Cantele, G.; Degoli, E.; Luppi, E.; Magri, R.; Ninno, D.; Iadonisi, G.; Ossicini, S. *Phys. Rev. B* **2005**, *72*, 113303.
(14) Ossicini, S.; Degoli, E.; Iori, F.; Luppi, E.; Magri, R.; Cantele, G.; Trani, F.; Ninno, D. *Appl. Phys. Lett.* **2005**, *87*, 173120
(15) Fong, C.-Y.; Zhong, H.; Klein, B. M.; Nelson, J. S. *Phys. Rev. B* **1994**, *49*, 7466.
(16) Lee, I.-H.; Ahn, K.-H.; Kim, Y.-H.; Martin, R. M.; Leburton, J.-P. *Phys. Rev. B* **1999**, *60*, 13720.
(17) Lannoo, M.; Delerue, C.; Allan, G. *Phys. Rev. Lett.* **1995**, *74*, 3415.
(18) (a) Hohenberg, P.; Kohn, W. *Phys. Rev.* **1964**, *136*, B864. (b) Kohn, W.; Sham, L. J. *Phys. Rev.* **1965**, *140*, A1135.
(19) Chelikowsky, J. R. *J. Phys. D: Appl. Phys.* **2000**, *33*, R33.
(20) Fujii, M.; Toshikiyo, K.; Takase, Y.; Yamaguchi, Y.; Hayashi, S. *J. Appl. Phys.* **2003**, *94*, 1990.
(21) Allan, G.; Delerue, C.; Lannoo, M.; Martin, E. *Phys. Rev. B* **1995**, *52*, 11982.
(22) Weil, J. A.; Bolton, J. R. *Electron Paramagnetic Resonance: Elementary Theory and Practical Applications*, 2nd ed.; Wiley: New Jersey, 2007.
(23) Van de Walle, C. G.; Blochl, P. E. *Phys. Rev. B* **1993**, *47*, 4244.
(24) The dielectric constant outside the nanocrystal should be one because the outside region is a vacuum. To simplify the analytical derivation that follows, the dielectric constant is made uniform throughout the whole space. Details outside of the nanocrystal should not have any significant effect on the results of the effective mass model. This is because the radius of the quantum well is approximately five times the effective Bohr radius a_B^{eff}; therefore, the tail of the defect wavefunction has small amplitude outside the nanocrystal.
(25) Penn, D. R. *Phys. Rev.* **1962**, *128*, 2093.
(26) (a) Brus, L. E. *J. Chem. Phys.* **1983**, *79*, 5566. (b) Brus, L. E. *J. Chem. Phys.* **1983**, *80*, 4403.

NL072997A